PHYSICAL REVIEW A VOLUME 56, NUMBER 3 SEPTEMBER 1997

Time-dependent evolution of an optical vortex in photorefractive media

A. V. Mamaev* and M. Saffman
Department of Optics and Fluid Dynamics, Risø National Laboratory, DK-4000 Roskilde, Denmark

A. A. Zozulya
JILA, Campus Box 440, University of Colorado, Boulder, Colorado 80309-0440
(Received 24 October 1996)

We study the transient decay and rotation of a singly charged optical vortex in media with a photorefractive nonlinearity under conditions where the light intensity is high compared to the saturation intensity. Transient decay of an initially circular vortex is characterized by charge-dependent rotation, and stretching of the vortex along the direction of the photogalvanic or externally applied field. When the medium reaches a steady state the effective nonlinearity at large times disappears and the vortex returns to its initial shape.
[S1050-2947(97)50909-7]

PACS number(s): 42.65.Sf, 42.65.Tg, 42.65.Hw

Three-dimensional solitary vortex solutions of the nonlinear Schrödinger equation were first considered in the context of superfluidity [1] and are an active topic in nonlinear optics [2]. It has been demonstrated experimentally that Kerr-type optical media with a cubic, isotropic, and local nonlinearity support stable (2+1)D vortex solitons that have radial symmetry [3]. Photorefractive materials offer the opportunity of studying soliton and vortex dynamics in nonlinear media with a response that is significantly different from that found in Kerr media. In the full three-dimensional case photorefractive media are anisotropic, and exhibit a nonlocal nonlinear response that is determined by the global distribution of the optical intensity [4,5]. The anisotropy leads to characteristic features of localized solitary solutions. In the case of a self-focusing nonlinearity the lowest-order solitary solutions are always elliptically shaped, with a transverse width that is narrowest along the anisotropy axis (direction of applied field) [6]. These solutions are intuitively reasonable generalizations of the radially symmetric solitary solutions found in isotropic Kerr-type media.

In the self-defocusing case studied here the situation is dramatically different. The radially symmetric vortex solutions observed in Kerr media [3] have no direct counterpart in photorefractives. By comparison with the self-focusing case one might naively expect to observe an elliptically shaped solitary vortex, with a fixed alignment relative to the anisotropy axis. However, the phase structure of the vortex implies that an elliptically shaped vortex core rotates as it propagates, so that it is impossible to maintain correct alignment. The result is that in the steady-state, and when the light intensity is comparable to the saturation intensity in the medium, excitation of the medium with a circular vortex leads to charge-dependent rotation, stretching, and eventual decay of the localized structure [7]. Another unique manifestation of the dominant role of anisotropy in photorefractive self-focusing is the recent experimental observation of the decay of a high-charge vortex [8]. The very existence of this decay is due to the anisotropy-driven stretching of the vortex core.

Nonetheless, the correct physical interpretation has been the subject of controversy since an earlier work [9] reported radially symmetric vortex solitons in photorefractive media. The reports of circular solitons [9] were, however, obtained in a transient regime, whereas the observations of vortex decay were obtained in the steady state [7]. Although the theory of nonlinear propagation in photorefractive media for both (1+1)D [10] and (2+1)D [4] geometries does not suggest any qualitative difference between the transient and steady-state responses, the question remains open as to whether such a difference might exist. We demonstrate here that the question may be answered in the negative, and that also under transient conditions vortex decay is observed.

The present paper analyzes the transient evolution of vortex beams in photorefractive media. It concentrates specifically on the region of parameters where the intensity of the light is considerably higher than the saturation intensity [for definitions see Eqs. (1)]. In this regime transient effects manifest themselves in the most clear and dramatic way. Our results show that transient evolution of the vortex results in its decay. This decay is characterized by charge-dependent rotation, and stretching of the vortex along the direction of the photogalvanic or externally applied field (the charge is the accumulated phase in multiples of 2π acquired in going around the vortex). If there exists no true steady state, or the transients last for an extremely long time (as in iron-doped $LiNbO_3$), the stretching proceeds unchecked, and results in a complete delocalization of the vortex. When the medium reaches a steady state (as in a photorefractive SBN crystal), the effective nonlinearity at large times disappears, and after a transient period of delocalization the vortex returns to its initial shape. The observed behavior agrees with and complements that seen previously under stationary conditions in a photorefractive SBN crystal with externally applied field [7]. The correspondence between the transient and stationary characteristics of the self-focusing is in agreement with the two- and three-dimensional theory for propagation in these media [10,4].

The experimental arrangement is shown in Fig. 1. A 30-mW He-Ne laser beam ($\lambda=0.63\ \mu$m) was diffracted from a computer-generated hologram to embed a unit charge vortex in the beam. The beam was then passed through a system

*Permanent address: Institute for Problems in Mechanics, Russian Academy of Sciences, Vernadsky Pr. 101, Moscow 117526, Russia.

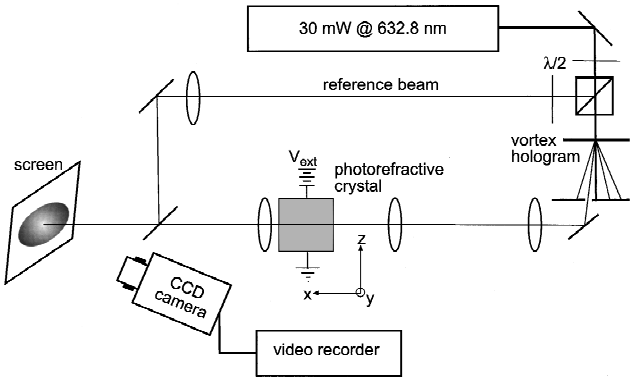

FIG. 1. Experimental setup.

of lenses to control the size of the beam at the input to the photorefractive medium. The beam was made to propagate perpendicular to the crystal c axis ($=z$ axis), and was polarized along it. Time-dependent images of the beam at the output face of the crystal were recorded with a charge-coupled-device (CCD) camera and video machine.

The results shown in Fig. 2. were obtained with a cube-shaped $LiNbO_3$ crystal doped with 0.03% Fe and measuring 5 mm along each side. The 100-μW input beam had an inner core diameter [full width at half maxium (FWHM)] of $d_v=22$ μm and an outer envelope diameter (FWHM) of $d_G=72$ μm. Frame 0 in Fig. 2 shows the initial distribution

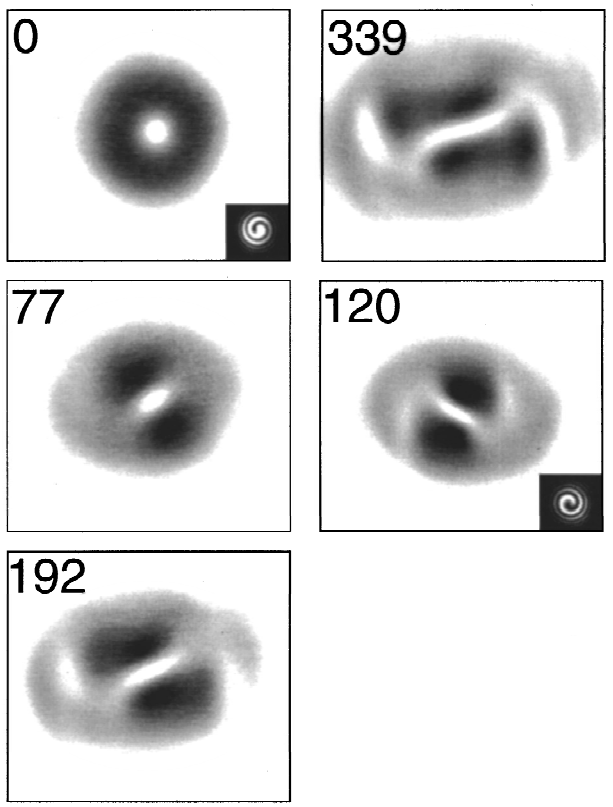

FIG. 2. Evolution of a charge-1 vortex in $LiNbO_3$ at times of 0, 77 192, and 339 sec. The final frame is for an oppositely charged vortex at 120 sec. The insets show interferograms demonstrating the sign of the input vortex. The pictures are negative images with low intensities represented by white regions, and the c axis is horizontal. Each frame depicts a region 175×155 μm.

of the output beam, obtained before the development of the photorefractive grating, characterized by $d_v=24$ μm and $d_G=79$ μm. The subsequent frames are labeled with the time in seconds. The nonlinearity results in transformation of the input circular vortex to one with elliptical core. The core is initially stretched along a line at a large angle to the z axis and subsequently rotates towards z. The core is simultaneously squeezed along the perpendicular direction. The redistribution of the field creates an intensity dip along the major axis; the field from the dip is pushed out along the positive and negative y axis (approximately), forming two lobes. The stretching proceeds unchecked, leading eventually to complete delocalization as seen in frame 192. At long times the beam acquires a complex structure of multiple bright and dark regions. The dark regions contain additional wavefront dislocations created in pairs [11] to preserve the total topological charge, as has been verified interferometrically. A similar decay into oppositely charged vortex pairs due to a polarization-induced anisotropy was predicted in [12]. The sign of rotation is determined by the vortex charge as demonstrated by the final frame, obtained with an input vortex of opposite charge. Similar behavior was observed using different input beam diameters and $LiNbO_3$ samples up to 1 cm in length and with higher and lower doping levels. The asymptotic rotation of the vortex core away from the c axis is smaller for the thicker samples.

Contours of the measured intensity at a time of 77 sec are shown in Fig. 3. The elliptical core seen at intermediate times may be characterized by two diameters: $d_{v\parallel}$ along the major axis of the ellipse and $d_{v\perp}$ along the minor axis. Using the value of the intensity at the peak of the lobes to define the FWHM diameters, we see that $d_{v\parallel}$ diverges.

The results shown in Fig. 4 were obtained with a crystal of SBN:60 doped with 0.002 wt % Ce. The crystal measured 10 mm along the direction of propagation, and was 10 mm wide along the $\hat{c}$ axis. The input beam power was 350 μW, and the beam dimensions were the same as for Fig. 2. A dc voltage of 700 V was applied along the $\hat{c}$ axis to control the value of the nonlinearity, and no additional backgound illumination was used. The largest effect is obtained at about 1.2 sec, while at 40 sec the nonlinearity has again disappeared. The final unlabeled frame shows the steady-state behavior with additional background illumination. There is no steady-state response without additional white-light background illumination to increase the photoconductivity.

In the theoretical analysis we use the following set of equations for the amplitude of the electric field B and the nonlinearly induced electrostatic potential φ [Ref. [4], Eq. (2) with $\chi=0$ and $\delta=0$]:

$$\left(\frac{\partial}{\partial x}-\frac{i}{2}\nabla^2\right)B=-i\frac{\partial\varphi}{\partial z}B, \tag{1a}$$

$$\vec{\nabla}\cdot\left[-\frac{\partial}{\partial t}(\hat{\epsilon}_n\vec{\nabla}\varphi)+I_T\left(-\vec{\nabla}\varphi+\vec{e}_z\frac{E_{\rm ext}}{\widetilde{E}}\right)+\alpha\vec{\nabla}I_T+\vec{e}_z\frac{E_{\rm ph}}{\widetilde{E}}I\right]=0, \tag{1b}$$

where $I_T=(1+I)/[1-\alpha\vec{\nabla}\cdot(\hat{\epsilon}_n\vec{\nabla}\varphi)]$, $I=|B|^2$ is the light intensity normalized to the saturation (dark and/or incoherent

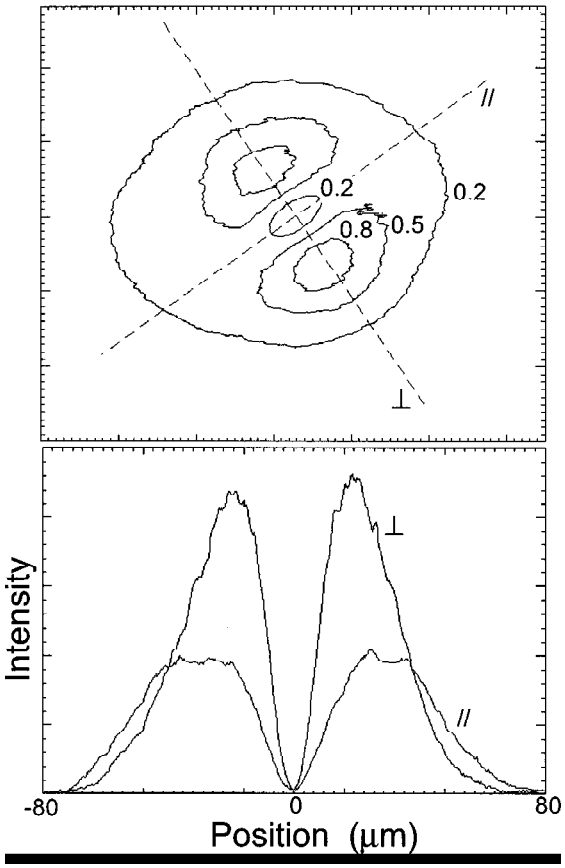

FIG. 3. Contours of the intensity distribution given in Fig. 2 at 77 sec. The contours are labeled with the fractional intensity relative to the peak and the profiles given below are along and perpendicular to the elliptical vortex core.

irradiation) intensity, and $\vec{\nabla}$ acts on the transverse coordinates y and z. The field is polarized along the z axis. The longitudinal coordinate is normalized to $l_{\|}=\lambda/\pi n^3 r_{33}\tilde{E}$ and the transverse ones to $l_{\perp}=(l_{\|}\lambda/2\pi n)^{1/2}$. Here n is the refractive index, r_{33} the relevant component of the electrooptic tensor, $\tilde{E}$ the characteristic internal field, E_{ext} the external electric field, E_{ph} the photogalvanic field, and $\hat{\epsilon}_n$ the static dielectric tensor normalized to the value of its ϵ_{33} component. $\alpha=1/k_D l_{\perp}$, where k_D is the Debye wave vector, is the measure of asymmetric contributions to the self-focusing or self-defocusing. The initial and boundary conditions for Eqs. (1) read $\varphi(t=0)=0$ and $\varphi(\infty)=0$.

A full time and space-dependent solution of Eqs. (1) is very computationally intensive. In the following we analyze the temporal dynamics of the refractive index induced by a light beam with an embedded vortex, assuming that the medium is thin and the field does not change appreciably [Eq. (1a) is not propagated]. The light field is taken as a doughnut mode $B\propto(r/d)\exp(-r^2/d^2+i\theta)$. The parameters are chosen such that the intensity distribution is an annular ring with the internal and external diameters equal to about 30 μm and 100 μm, respectively. The maximum intensity of the beam I_m is taken to be equal to 100, the ratio $E_{\text{ext}}/\tilde{E}=1$, $E_{\text{ext}}=0.7$ kV/cm, and $E_{\text{ph}}=0$.

Figure 5 shows cross sections of the nonlinear refractive index $\nu=\partial\varphi/\partial z$ along the z (solid) and y (dashed curves)

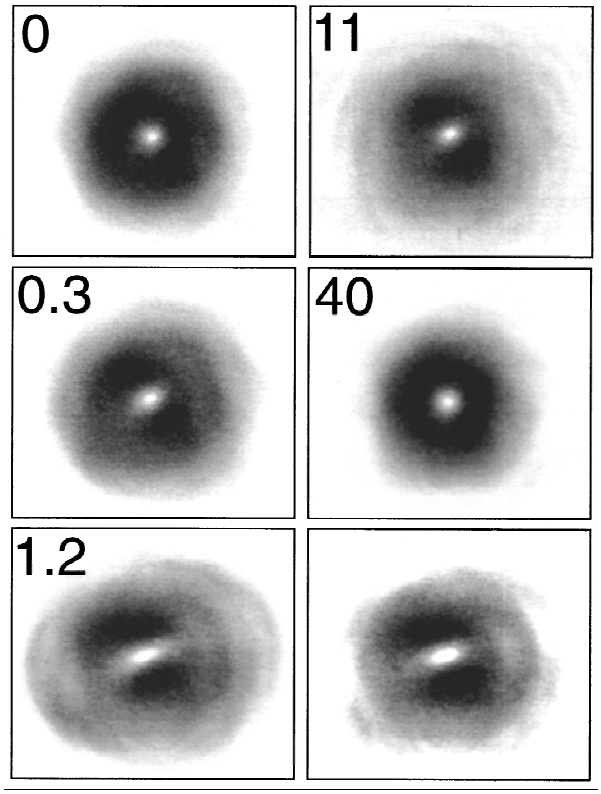

FIG. 4. Evolution of a charge-1 vortex in SBN at times of 0, 0.3, 1.2, 11, and 40 sec. The final frame shows the steady-state behavior with background illumination. Each frame depicts a region 175 $\times$150 μm.

coordinates taken through the center of the intensity distribution ($y=0,z=0$) as functions of time. The time is normalized to that corrersponding to the maximum intensity $I_m=100$.

At zero time $t=0$ the change in the refractive index is zero. At the initial stage of evolution ($t=0.1$ in Fig. 5) the

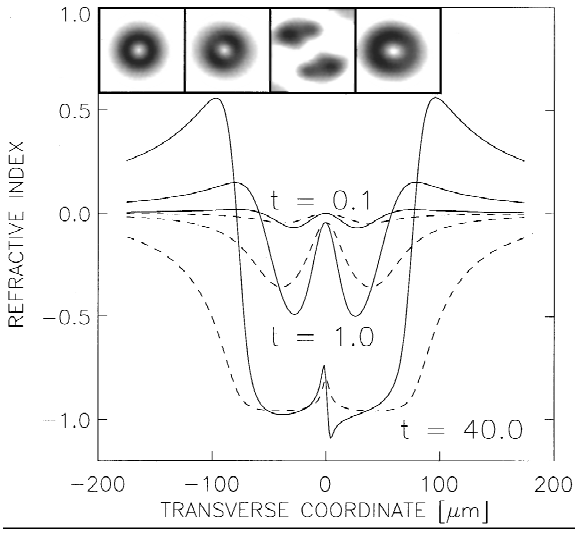

FIG. 5. Temporal development of the nonlinear part of the refractive index along the z and y coordinates. The solid and dashed lines show the variation along z and y, respectively. The insets show the corresponding far-field intensity distributions (negative images).

refractive index grows approximately proportional to the local intensity, though from the very beginning it is already anisotropic. The bulk of the refractive index corresponds to a negative lens and results in the defocusing of the beam as a whole but the central part forms a potential well for the embedded vortex. This stage corresponds roughly to the frame 0.3 in Fig. 4. At moderate times the magnitude of the refractive index keeps growing and the depth of the potential well in the center increases ($t=1.0$). At the end of this intermediate stage the nonlinear focusing effects for the vortex are at their maximum (frame 1.2 in Fig. 4). At still larger times the effective nonlinearity responsible for focusing of the vortex and defocusing of the main beam starts decreasing. The asymptotic steady-state distribution of the refractive index is given by the curves corresponding to $t=40$. It demonstrates a strong decrease in the depth and the width of the potential well for the vortex as compared to the intermediate times. Combined with the flattened top of the refractive index distribution it results in near disappearance of focusing and/or defocusing properties of the medium for the light beam that created this distribution. This is confirmed by the far-field intensity distributions of light shown in Fig. 5. The four frames correspond to times $t=0$, 0.1, 1.0, and 40.0, respectively. In the limit $I_m \to \infty$ the effective focusing or defocusing properties of the nonlinearity completely vanish in the steady state. This is seen clearly in the last experimental frame labeled 40 in Fig. 4.

The physical reason for the decrease of the nonlinearity in the steady state can be explained in the following way: the conductivity of the medium is proportional to the concentration of free charges generated by the beam. The rate of their generation is proportional to the local intensity of the beam, but once generated, they can move by drift and/or diffusion. When the light intensity is much larger than the saturation intensity, the conductivity inside the beam is very high as compared to the rest of the crystal. Any external field necessary to produce a focusing or defocusing response is screened out and cannot penetrate into the bulk of the beam. The screening takes place as soon as the generated charges have time to redistribute themselves and form two opposite-sign layers of charge on both sides of the main beam along the z axis, in the regions where its intensity becomes comparable to the saturation intensity (see [4,10] for the corresponding pictures in the focusing case). At large beam-to-saturation intensity ratios the screening is very strong and the effective nonlinearity decreases dramatically as compared to its value at an intermediate stage.

The sharp antisymmetric jump in the refractive index close to the origin of coordinates at $t=40$ is due to the terms proportional to the parameter α in Eq. (1). These terms result in the asymmetric part of the material response and are responsible for the stimulated incoherent scattering (fanning) of a large-size beam. Its physical reason is the formation of triple charge layers in the region where the local beam intensity is of the order of the saturation intensity. Similar jumps have been discussed in connection with fanning in Ref. [13].

In summary we have demonstrated time-dependent stretching, rotation, decay, and possible return to the initial state of a unit charge optical vortex in photorefractive media with nonlinearity due to a photogalvanic or externally applied field. In the case of an externally applied field (Fig. 4) the medium reaches a true steady state and the vortex returns to its initial shape when the nonlinearity effectively goes to zero because of the screening. The photogalvanic media in our experiments never reach a true steady state. The evolution of the vortex in this case (Fig. 2) results in its complete delocalization and formation of additional vortex pairs. The above behavior suggests that even in the first case under appropriate conditions it may be possible to observe the decay of a vortex beyond stretching and rotation, into a structure of several vortex pairs, followed by a recovery at long time, with disappearance of the nonlinearity.

The authors would like to thank B. Fornberg for helpful discussions concerning numerics and E. Rasmussen for preparing the holographic mask. This work was supported by the Danish Natural Science Research Council. A.A.Z. acknowledges the support of the U.S. National Science Foundation Optoelectronics Computing Center, an NSF Engineering Research Center.

[1] V. L. Ginzburg and L. P. Pitaevskii, Zh. Éksp. Teor. Fiz. **34**, 1240 (1958) [Sov. Phys. JETP **34**, 858 (1958)].

[2] Yu S. Kivshar, IEEE J. Quantum Electron. **28**, 250 (1993); C. O. Weiss, Phys. Rep. **219**, 311 (1992); K. Staliunas, Chaos Solitons Fractals **4**, 1783 (1994).

[3] G. A. Swartzlander, Jr. and C. T. Law, Phys. Rev. Lett. **69**, 2503 (1992).

[4] A. A. Zozulya and D. Z. Anderson, Phys. Rev. A **51**, 1520 (1995).

[5] N. Korneev *et al.*, J. Mod. Opt. **43**, 311 (1996).

[6] A. A. Zozulya, D. Z. Anderson, A. V. Mamaev, and M. Saffman, Europhys. Lett. **36**, 419 (1996).

[7] A. V. Mamaev, M. Saffman, and A. A. Zozulya, Phys. Rev. Lett. **77**, 4544 (1996).

[8] A. V. Mamaev, M. Saffman, and A. A. Zozulya, Phys. Rev. Lett. **78**, 2108 (1997).

[9] G. Duree *et al.*, Phys. Rev. Lett. **74**, 1978 (1995).

[10] A. A. Zozulya and D. Z. Anderson, Opt. Lett. **20**, 837 (1995).

[11] A. V. Ilyenkov *et al.*, Appl. Phys. B **62**, 465 (1996).

[12] C. T. Law and G. A. Swartzlander, Jr., Chaos Solitons Fractals **4**, 1759 (1994).

[13] A. A. Zozulya and D. Z. Anderson, Phys. Rev. A **52**, 878 (1995).